Supplementary information for

Strain-invariant near-zero Poisson's ratio emerging in 2D $(CuX)_2P_8Se_3$ (X=Br, I) hybrid structures

Xingxu Meng,[a] Minglei Jia,[a,b] Huimin Shen,[c] and Huabing Yin[a,*]

[a]*Institute for Computational Materials Science, Henan Key Laboratory of High Efficiency Energy Conversion Science and Technology, and Henan International Joint Laboratory of New Energy Materials and Devices, School of Physics and Electronics, Henan University, Kaifeng 475004, China*

[b]*School of Electro-Mechanical Engineering, Zhongyuan Institute of Science and Technology, Xuchang 461000, China*

[c]*College of Intelligent Science and Engineering, Yantai Nanshan University, Yantai 265713, China*

[*] Corresponding author.

E-mail addresses: yhb@henu.edu.cn (Huabing Yin)

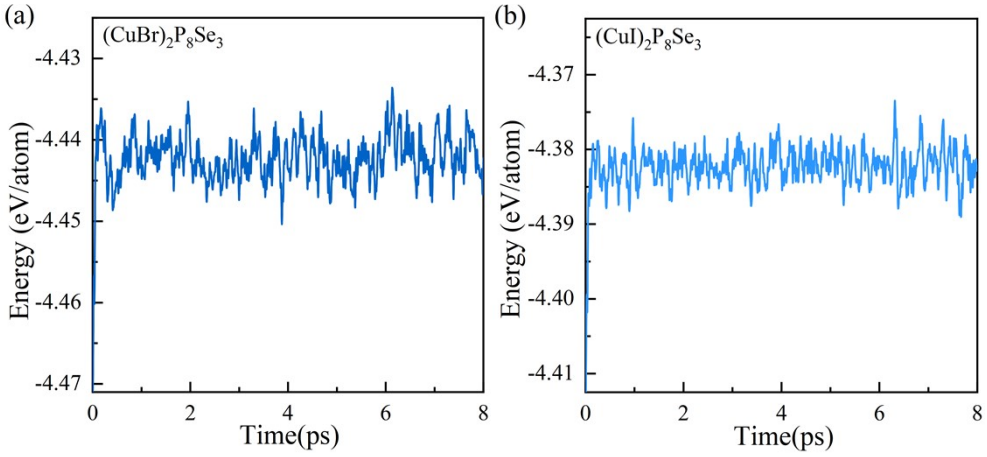

Fig. S1. The fluctuation of total energy of (a) $(CuBr)_2P_8Se_3$ and (b) $(CuI)_2P_8Se_3$ monolayers simulated with AIMD at 300 K.

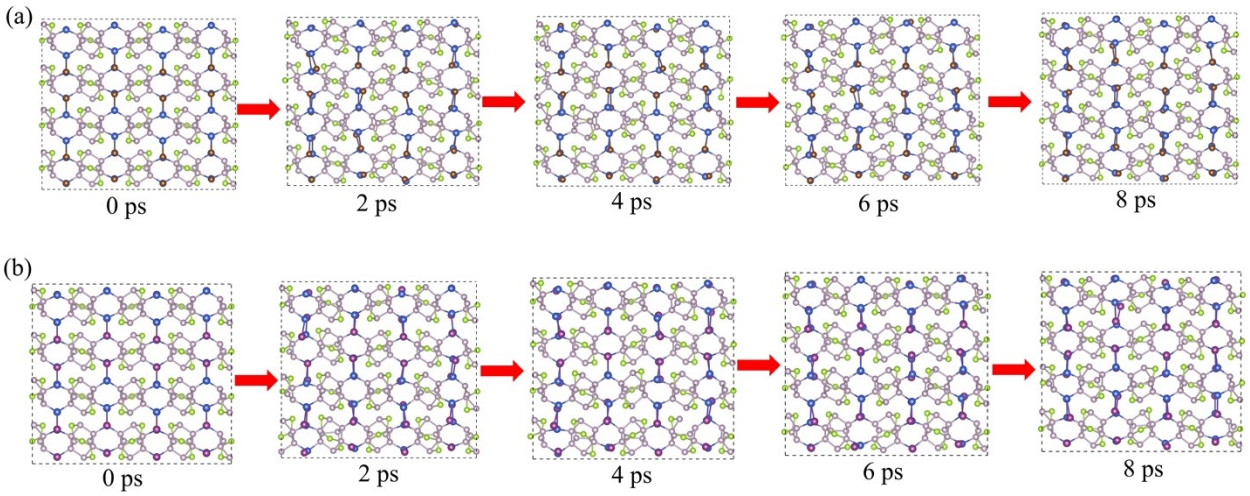

Fig. S2. The representative snapshots of (a) $(CuBr)_2P_8Se_3$ and (b) $(CuI)_2P_8Se_3$ monolayers simulated with AIMD at 300 K.

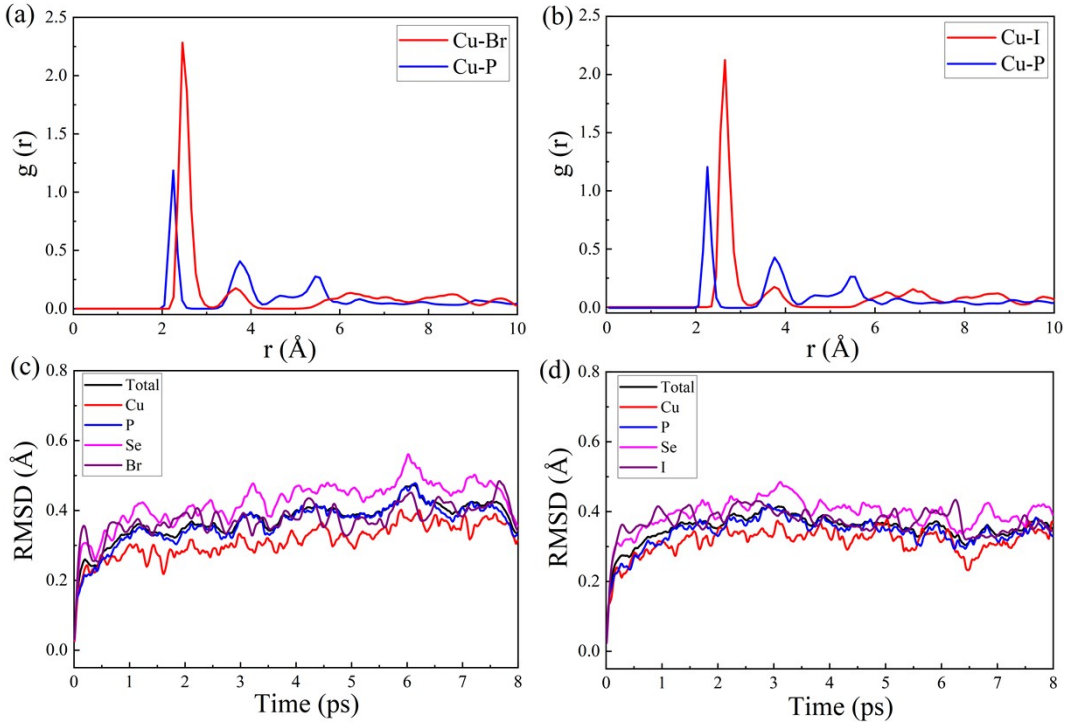

Fig. S3. The radial distribution function (RDF) and root-mean-square deviation (RMSD) of (a, c) $(CuBr)_2P_8Se_3$ and (b, d) $(CuI)_2P_8Se_3$ monolayers over the AIMD simulation period.

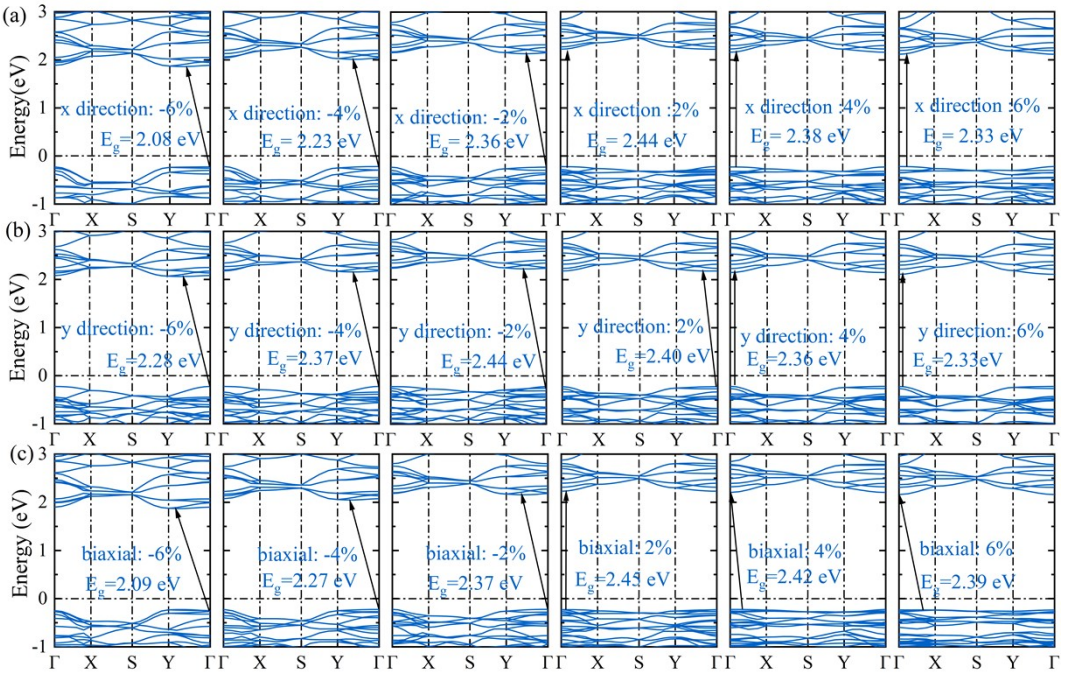

Fig. S4. Band structures of the $(CuBr)_2P_8Se_3$ monolayer under in-plane (a) and (b) uniaxial and (c) biaxial strains varying from 6% to 6%. The HSE06 functional is used in the calculations and the bandgaps are highlighted in black.

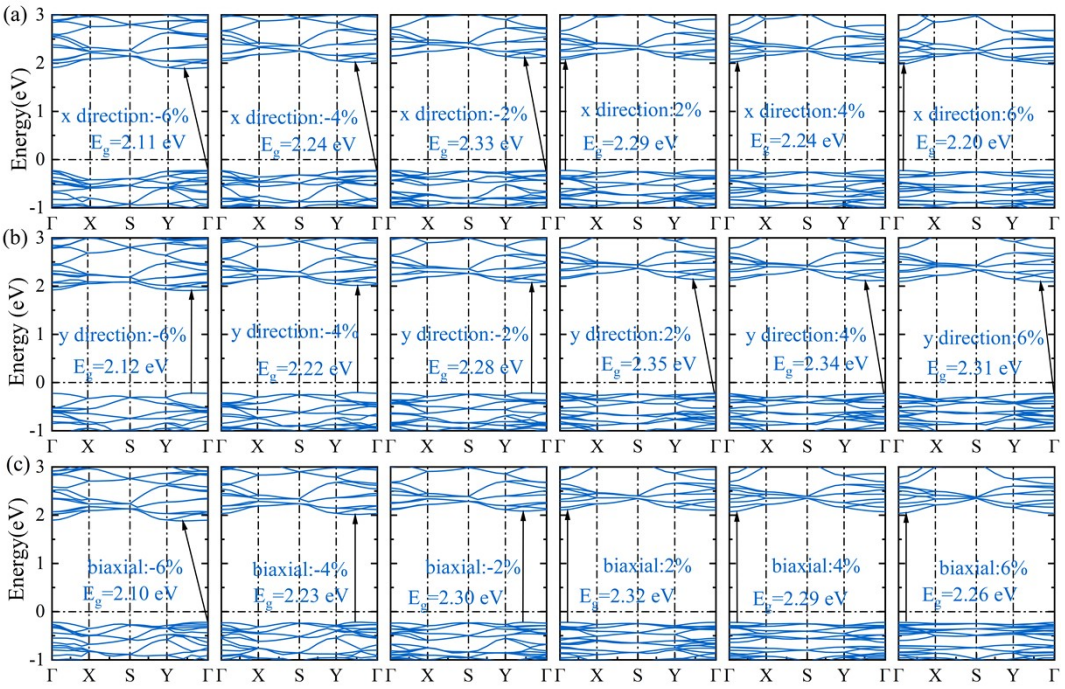

Fig. S5. Band structures of the $(CuI)_2P_8Se_3$ monolayer under in-plane (a) and (b) uniaxial and (c) biaxial strains varying from 6% to 6%. The HSE06 functional is used in the calculations and the bandgaps are highlighted in black.

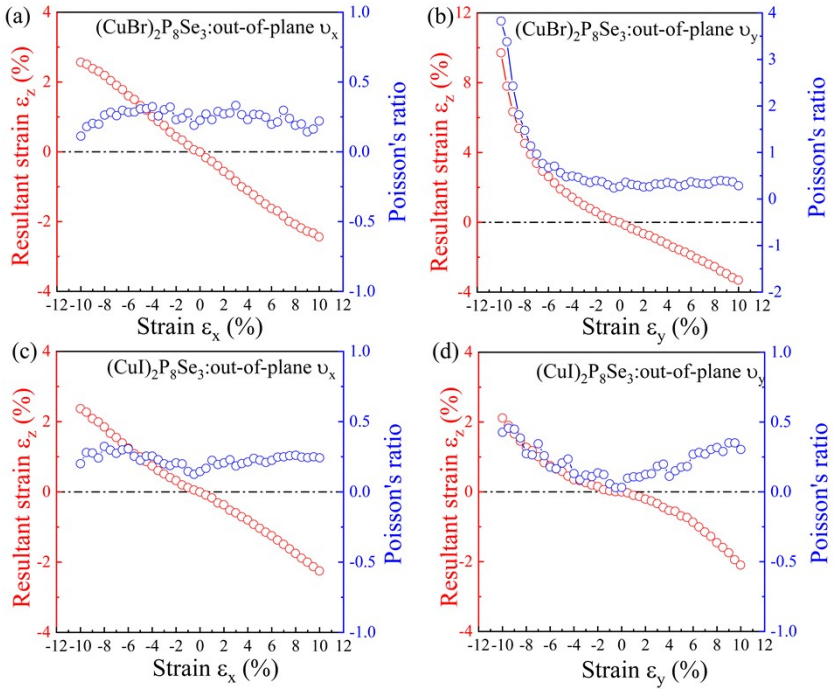

Fig. S6. The out-of-plane mechanical responses of the (a, b) $(CuBr)_2P_8Se_3$ and (c, d) $(CuI)_2P_8Se_3$ monolayer under uniaxial strain along the *x* and *y* directions, respectively.

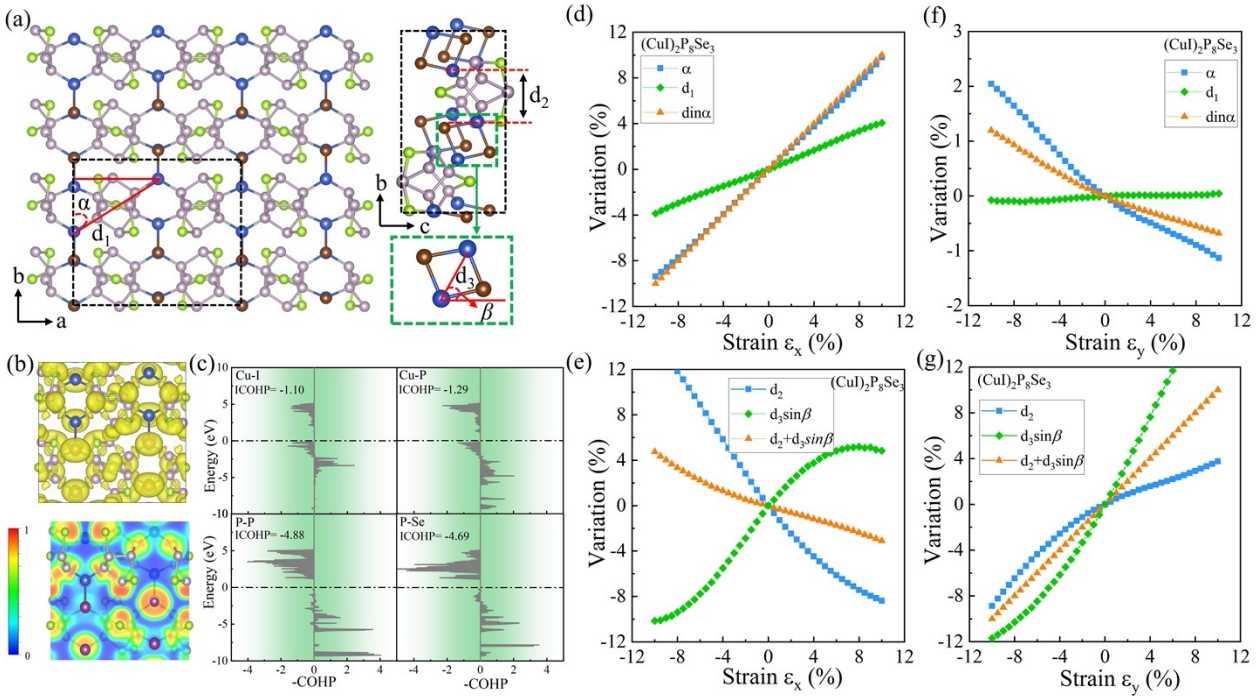

Fig. S7. (a) The definition of in-plane geometrical parameters of the $(CuI)_2P_8Se_3$ monolayer: distances d_1, d_2, and d_3 and angles α and β. (b) The 3D and 2D electron localization function (ELF) of the $(CuI)_2P_8Se_3$ monolayer. (c)

The negative crystal orbital Hamilton population (−COHP) of the local bonds in monolayer $(CuI)_2P_8Se_3$: Cu–I, Cu–P, P–P, and P–Se bonds. The corresponding integrated COHP (ICOHP) values for these bonds are also presented. The dashed line represents the Fermi level. The evolution of the key geometrical parameters with respect to the applied strains along the (d, e) *x* and (f, g) *y* directions, respectively.